

# Simple Model and Predictive Control of a Pharmaceutical Batch Fluidized Bed Dryer

Francis Gagnon\* André Desbiens\* Éric Poulin\*  
Jocelyn Bouchard\* Pierre-Philippe Lapointe-Garant\*\*

\* *Process Observation and Optimization Laboratory (LOOP),  
Université Laval, Quebec City, G1V 0A6, Canada*

\*\* *Process Monitoring Automation and Control group (PMAC), Pfizer  
Canada ULC, Montreal, H9J 2M5, Canada*

---

**Abstract:** The fluidized bed theory can be complex, especially for heterogeneous flow descriptions with bypasses, generally resulting in large differential and algebraic systems of equations. Consequently, their applicability to model-based process control is limited. In this work, a simplified homogeneous model for pharmaceutical batch drying is derived from the two-phase fluidization theory using physical insights and simplifying assumptions, reducing more than a hundred equations to five. A nonlinear model predictive controller with an internal model structure is designed from these simple equations, showing the simplicity of tuning and implementation. Parameters of the model are calibrated through nonlinear grey-box identification using pilot scale experimental data. The validation demonstrates that the proposed simplifications do not impair the ability to replicate the process dynamics adequately with experimental conditions similar to the ones used for calibration. Closed-loop results in simulation attest the robustness of this control strategy.

*Keywords:* Modeling and Identification, Model-based Control, Batch Processes

---

## 1. INTRODUCTION

The intense particle mixing and heat diffusivity of fluidized beds explains their popularity for pharmaceutical product drying. However, the gas flow through fluidized solids follows heterogeneous patterns with bypasses, generally perceptible as gas bubbles (Yang, 2003). Consequently, theories describing fluidized bed gas behavior are complex, leading to mathematical models hardly applicable for actual industrial developments (Philippsen et al., 2015). This is the case for process control design and implementation because computational burdens and tuning complexity hinder real-time applications (e.g. Gagnon et al., 2017). Simplifying the fluidized bed dryer (FBD) dynamic model is thus desirable, at the very least for control purposes.

Burgschweiger et al. (1999) and Gagnon et al. (2020) introduce two-phase batch FBD models to describe gas flow patterns. Although more realistic than single-phase descriptions (Dry and Judd, 1985), they generally lead to large differential and algebraic equation systems requiring complex solving workflow.

A homogeneous single-phase dryer with nonuniform distributions for internal moisture in particles is described in Martinez-Vera et al. (1995). Distributed models cannot be applied in a straightforward manner to process control. Alternatively, the van Meel normalization (van Meel, 1958) or the characteristic drying curves concepts (Mujumdar, 2014) enable a lumped description of sorption and internal diffusion kinetics, like the single-phase model of Gavi (2019). Separate experimentation is however required to determine the curve function, the critical, and the equi-

librium moisture content. Furthermore, these parameters depend on inlet conditions and experimental equipment (Mujumdar, 2014). A homogeneous representation is described in Syahrul et al. (2003), but simulations need outlet gas data as inputs. It must also be emphasized that an accurate sorption model is less crucial for applications dominated by the constant rate period (or first drying stage), which is common for pharmaceutical product.

Other approaches include purely empirical or black-box models. However, incorporating the inlet gas condition effect in these strategies is difficult and ambiguous since impacts on empirical parameter values are not well-defined (Mujumdar, 2014). This feature is essential for process control applications since the gas feed rate and temperature are the main manipulated inputs during drying. Linear model identification and control are also not trivial since batch processes like FBDs cannot be linearized around an operating point and exhibit irreversible reactions (Nagy and Braatz, 2003). These features explain why their dynamics are generally classified as highly nonlinear and less suitable for classical control.

This paper presents a simple predictive controller for batch FBDs based on a single-phase model. To this end, the two-phase equations of Gagnon et al. (2020) are reduced using simplifying assumptions and physical approximations. They are then used for nonlinear model predictive control (NMPC) based on an internal model scheme, leading to an algorithm relatively easy to implement and tune. The model parameters are calibrated with a nonlinear grey-box identification algorithm on pharmaceutical pilot scale data. The validation compares simulations with the

complete two-phase description on separate dataset. Implementing the control strategy on a simulated two-phase FBD attests closed-loop performance and robustness.

## 2. MATERIALS AND METHODS

The single-phase model is first derived from the comprehensive model of Gagnon et al. (2020) using approximate assumptions and conservation laws. Refer to this paper for information on equipment and measurements, since the data presented here are the same. The control algorithm is briefly described afterward. The objective is to reach a particle moisture content setpoint at the end of the batch while keeping a maximum product temperature constraint.

### 2.1 Model Assumptions

Gagnon et al. (2020) is based on the two-phase theory (Kunii and Levenspiel, 1991). It involves more than a hundred equations. The assumptions introduced hereafter are used to simplify the model. It is acknowledged that some of them have a questionable validity. However, control applications only require general trends since the feedback loop can handle modeling errors to some extent. The neglected phenomena can also impact parameter values during grey-box identification.

- The fluidized bed is seen as a perfectly homogeneous mix of interstitial gas and particles, called the emulsion, with constant void fraction and batch size. There are no bubbles, gas bypasses and heat losses in the bed (adiabatic process).
- Variations of physical properties of components with temperature, pressure and moisture are neglected.
- Steady-state is assumed for mass and heat transfers on gaseous control volumes.
- The vapor sensible heat is considered negligible compared to the latent heat.
- Particle size distribution is neglected, the particles are small, and their volume is invariant during drying. They all have the same physical properties, moisture content, and temperature at a given time during the drying and there is no interaction between them.
- The solid material is supposed non-hygroscopic. The drying kinetics are divided into two distinct stages. The constant rate period assumes vapor-saturated stagnant films around the particles. The particle internal moisture vaporizes during the following falling rate period. A simplified version of characteristic drying curves is used, needing no separate experiments.
- The inlet air moisture content is constant and its influence in the total airflow rate is neglected. First order dynamics and direct transmission are assumed for the closed-loop responses of the inlet temperature and airflow, respectively.

In this work, fluctuations in inlet air moisture are not taken into account during modeling and handled by the feedback.

### 2.2 Mass Balance

From Gagnon et al. (2020) two-phase model, the particle mass balance equation at time  $t$  is:

$$\rho_{pd} \frac{d\chi_p}{dt} = -\frac{6}{\phi d_p} k_{pf,e} \rho_g (\chi_{pf} - \chi_e) \quad (1)$$

with  $\chi_p$ ,  $\chi_{pf}$  and  $\chi_e$  being the dry basis moisture content of the particles, the stagnant gas film around them, and the interstitial gas, respectively. Particles have a size  $d_p$ , sphericity  $\phi$  and dry skeletal density  $\rho_{pd}$ .  $k_{pf,e}$  is the mass transfer coefficient with the interstitial gas, and  $\rho_g$ , the air density. The steady-state mass balance of the interstitial gas is:

$$\frac{v_{mf}}{z_f} (\chi_e - \chi_0) = \frac{6(1 - \varepsilon_f)}{\phi d_p} k_{pf,e} (\chi_{pf} - \chi_e) - \delta \mathcal{K}_{e,b} (\chi_e - \tilde{\chi}_b) \quad (2)$$

with  $\chi_0$  and  $\tilde{\chi}_b$  as the inlet gas moisture content and the bubble phase space-average value, respectively. The dry air velocity and the void fraction of the interstitial gas are supposed fixed at the minimum fluidization values  $v_{mf}$  and  $\varepsilon_{mf}$ . The fluidized bed height  $z_f$  and total void fraction  $\varepsilon_f$  depend on the bubble phase volume fraction  $\delta$ . A single-phase or homogeneous model is obtained from (2) by setting the bubble fraction at  $\delta = 0$ . Also, the dry velocity of the interstitial gas is no longer fixed at  $v_{mf}$ , but rather follows the inlet value  $v_0$ . Hence, the interstitial gas mass balance in a single-phase form is:

$$\frac{v_0}{z_f} (\chi_e - \chi_0) = \frac{6(1 - \varepsilon_f)}{\phi d_p} k_{pf,e} (\chi_{pf} - \chi_e) \quad (3)$$

On dryers typically,  $\chi_0$  is low enough to simplify with  $v_0 = \dot{V}_0 / [S_f(1 + \chi_0)] \approx \dot{V}_0 / S_f$ , giving:

$$\frac{\dot{V}_0}{S_f z_f} (\chi_e - \chi_0) = \frac{6(1 - \varepsilon_f)}{\phi d_p} k_{pf,e} (\chi_{pf} - \chi_e) \quad (4)$$

with  $\dot{V}_0$ , the inlet volumetric flow rate, and  $S_f$ , the fluidized bed cross-sectional area.

By introducing the coefficient  $a_2$  defined as:

$$a_2 = \frac{6k_{pf,e}\rho_g}{\phi d_p \rho_{pd}} \quad (5)$$

equation (1) becomes:

$$\frac{d\chi_p}{dt} = a_2 (\chi_e - \chi_{pf}) \quad (6)$$

For moderate airflow variations,  $z_f$  and  $\varepsilon_f$  can be supposed constants (fixed batch size with a constant fluidized bed expansion). By introducing  $a_3$  and  $a_4$  defined as:

$$a_3 = \frac{1}{S_f z_f} \quad \text{and} \quad a_4 = \frac{6(1 - \varepsilon_f)k_{pf,e}}{\phi d_p} \quad (7)$$

equation (4) transforms into:

$$\chi_e = \frac{a_3 \dot{V}_0}{a_3 \dot{V}_0 + a_4} \chi_0 + \frac{a_4}{a_3 \dot{V}_0 + a_4} \chi_{pf} \quad (8)$$

Inserting (8) into (6) and simplifying give:

$$\frac{d\chi_p}{dt} = \frac{a_2 a_3 \dot{V}_0}{a_3 \dot{V}_0 + a_4} (\chi_0 - \chi_{pf}) \quad (9)$$

When particles are small ( $d_p < 100 \mu\text{m}$ ), the coefficient  $a_4$  is at least three orders of magnitude larger than  $a_3 \dot{V}_0$ . This observation enables the simplification  $1/(a_3 \dot{V}_0 + a_4) \approx 1/a_4$ , giving:

$$\frac{d\chi_p}{dt} = \frac{a_2 a_3 \dot{V}_0}{a_4} (\chi_0 - \chi_{pf}) \quad (10)$$

Introducing the gas-particle mass transfer ratio per unit volume of fluidized bed  $a_1$ :

$$a_1 = \frac{a_2 a_3}{a_4} = \frac{\rho_g}{\rho_{pd} S_f z_f (1 - \varepsilon_f)} \quad (11)$$

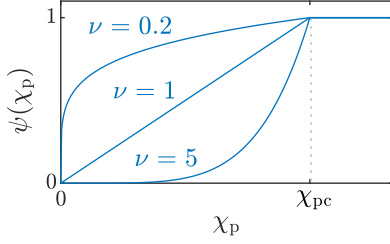


Fig. 1. Possible falling rate correction curves

the mass balance becomes:

$$\frac{d\chi_p}{dt} = a_1 \dot{V}_0 (\chi_0 - \chi_{pf}) \quad (12)$$

The moisture content of the particle gas film  $\chi_{pf}$  can be estimated with:

$$\chi_{pf} = \gamma(T_p) \psi(\chi_p) \quad (13)$$

Assuming non-hygroscopic particles,  $\gamma(T_p)$  is related to the saturation mixing ratio  $\chi_{sat}$ . Since the temperature range is relatively narrow, it can be estimated with an exponential relation:

$$\gamma(T_p) = \alpha \exp(\beta T_p) \quad (14)$$

with shape modification parameters  $\alpha$  and  $\beta$ . The film is no longer saturated in the falling rate period as moisture needs to diffuse from the particle internal pores to surface to vaporize. Similarly to the characteristic drying curve concept (Mujumdar, 2014), an empirical correction function is used here. By normalizing with the critical moisture content  $\chi_{pc}$  only (neglecting the equilibrium value here), a simple correction function is:

$$\psi(\chi_p) = \begin{cases} 1 & \frac{\chi_p}{\chi_{pc}} \geq 1 \\ \left(\frac{\chi_p}{\chi_{pc}}\right)^\nu & \frac{\chi_p}{\chi_{pc}} < 1 \end{cases} \quad (15)$$

with the exponent  $\nu$  controlling the curvature induced by the particle sorption characteristic, as depicted in Fig. 1. The final form of the simplified mass balance is therefore:

$$\frac{d\chi_p}{dt} = a_1 \dot{V}_0 [\chi_0 - \gamma(T_p) \psi(\chi_p)] \quad (16)$$

### 2.3 Energy Balance

From Gagnon et al. (2020), the energy balance of the particles at temperature  $T_p$  is:

$$\rho_{pd}(c_s + \chi_p c_w) \frac{dT_p}{dt} = \frac{6}{\phi d_p} \left\{ h_{e,pf}(T_e - T_p) - k_{pf,e} \rho_g \right. \\ \left. \times (\chi_{pf} - \chi_e) [\Lambda_{wv} + (c_{wv} - c_w)(T_p - T_{wv})] \right\} \quad (17)$$

where  $h_{e,pf}$  is the heat transfer coefficient from the interstitial gas, and  $c_s$ ,  $c_w$  and  $c_{wv}$ , the specific heat capacities of the solid material, water and vapor respectively. By neglecting the water contribution in the particle enthalpy and the vapor sensible heat  $c_{wv} \Delta T$  relative to the vaporization latent heat  $\Lambda_{wv}$ , i.e. setting  $c_w = c_{wv} = 0$  here, equation (17) becomes:

$$\frac{dT_p}{dt} = \frac{6h_{e,pf}}{\phi d_p \rho_{pd} c_s} (T_e - T_p) - \frac{6k_{pf,e} \rho_g}{\phi d_p \rho_{pd} c_s} (\chi_{pf} - \chi_e) \Lambda_{wv} \quad (18)$$

Defining  $a_5$  and  $a_6$  as:

$$a_5 = \frac{6h_{e,pf}}{\phi d_p \rho_{pd} c_s} \quad \text{and} \quad a_6 = \frac{6k_{pf,e} \rho_g \Lambda_{wv}}{\phi d_p \rho_{pd} c_s} \quad (19)$$

the energy balance can be rewritten as:

$$\frac{dT_p}{dt} = a_5 (T_e - T_p) + a_6 (\chi_e - \chi_{pf}) \quad (20)$$

The interstitial gas steady-state energy balance is :

$$\frac{v_{mf}}{z_f} (c_g + \chi_0 c_{wv}) (T_e - T_0) = \frac{\delta \mathcal{H}_{b,e}}{\rho_g} (\tilde{T}_b - T_e) \\ + \frac{6(1 - \varepsilon_f)}{\phi d_p} \left\{ k_{pf,e} (\chi_{pf} - \chi_e) c_{wv} + \frac{h_{e,pf}}{\rho_g} \right\} (T_p - T_e) \\ - \frac{4h_{e,v}}{d_v \rho_g} (T_e - T_v) \quad (21)$$

By transforming the equation into a single-phase model ( $\delta = 0$  and  $v_{mf} = v_0$ ), neglecting heat loss through the vessel with  $h_{e,v} = 0$ , replacing the dry air velocity with  $v_0 \approx \dot{V}_0 / S_f$ , and neglecting the vapor sensible heat ( $c_{wv} = 0$ ), the energy balance simplifies to:

$$\frac{\dot{V}_0}{z_f S_f} c_g (T_e - T_0) = \frac{6(1 - \varepsilon_f) h_{e,pf}}{\phi d_p \rho_g} (T_p - T_e) \quad (22)$$

Introducing  $a_7$  and  $a_8$  as:

$$a_7 = \frac{c_g}{z_f S_f} \quad \text{and} \quad a_8 = \frac{6(1 - \varepsilon_f) h_{e,pf}}{\phi d_p \rho_g} \quad (23)$$

and rearranging (22) leads to:

$$T_e = \frac{a_7 \dot{V}_0}{a_7 \dot{V}_0 + a_8} T_0 + \frac{a_8}{a_7 \dot{V}_0 + a_8} T_p \quad (24)$$

Inserting (24) and (8) into the particle energy balance of (20) yields to:

$$\frac{dT_p}{dt} = \frac{a_5 a_7 \dot{V}_0}{a_7 \dot{V}_0 + a_8} (T_0 - T_p) + \frac{a_6 a_3 \dot{V}_0}{a_3 \dot{V}_0 + a_4} (\chi_0 - \chi_{pf}) \quad (25)$$

For small particles, the equation can be further simplified with  $1/(a_3 \dot{V}_0 + a_4) \approx 1/a_4$  and  $1/(a_7 \dot{V}_0 + a_8) \approx 1/a_8$  like the mass balance, giving:

$$\frac{dT_p}{dt} = \frac{a_5 a_7 \dot{V}_0}{a_8} (T_0 - T_p) + \frac{a_6 a_3 \dot{V}_0}{a_4} (\chi_0 - \chi_{pf}) \quad (26)$$

By introducing  $b_1$  and  $b_2$  coefficients as:

$$b_1 = \frac{a_6 a_3}{a_4} = \frac{\rho_g \Lambda_{wv}}{\rho_{pd} S_f z_f (1 - \varepsilon_f) c_s} \quad (27)$$

$$b_2 = \frac{a_5 a_7}{a_8} = \frac{\rho_g c_g}{\rho_{pd} S_f z_f (1 - \varepsilon_f) c_s} \quad (28)$$

and substituting  $\chi_{pf}$  with (13), the energy balance simplifies to its final form:

$$\frac{dT_p}{dt} = b_1 \dot{V}_0 [\chi_0 - \gamma(T_p) \psi(\chi_p)] + b_2 \dot{V}_0 [T_0 - T_p] \quad (29)$$

Empirical coefficients  $b_1$  and  $b_2$  represent the gas-particle energy transfer ratios per unit volume of fluidized bed.

### 2.4 Inlet Heater and Blower

The dryer inlet airflow and temperature are normally controlled. Relative to drying dynamics, the closed-loop performance of the airflow loop is typically fast enough to assume a direct transmission between the setpoint  $\dot{V}_{sp}$  and process value  $\dot{V}_0$ :

$$\dot{V}_0 \approx \dot{V}_{sp} \quad (30)$$

The transient response between the inlet temperature setpoint  $T_{sp}$  and process value  $T_0$  is supposed to exhibit first order dynamics with unity gain:

$$\frac{dT_0}{dt} = (1/\tau) [T_{sp} - T_0] \quad (31)$$

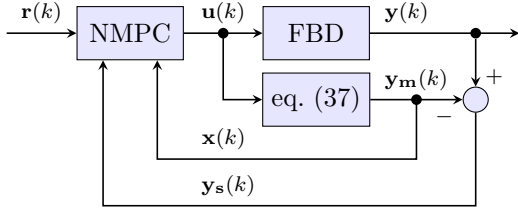


Fig. 2. Nonlinear predictive control with internal model with  $\tau$  representing the heater closed-loop time constant.

### 2.5 State-Space Representation

Combining (14)–(16) and (29)–(31), the model is:

$$\frac{dT_0}{dt} = (1/\tau) [T_{sp} - T_0] \quad (32)$$

$$\frac{d\chi_p}{dt} = a_1 \dot{V}_{sp} [\chi_0 - \gamma(T_p)\psi(\chi_p)] \quad (33)$$

$$\frac{dT_p}{dt} = b_1 \dot{V}_{sp} [\chi_0 - \gamma(T_p)\psi(\chi_p)] + b_2 \dot{V}_{sp} [T_0 - T_p] \quad (34)$$

with

$$\gamma(T_p) = \alpha \exp(\beta T_p) \quad (35)$$

$$\psi(\chi_p) = \begin{cases} 1 & \frac{\chi_p}{\chi_{pc}} \geq 1 \\ \left(\frac{\chi_p}{\chi_{pc}}\right)^\nu & \frac{\chi_p}{\chi_{pc}} < 1 \end{cases} \quad (36)$$

where  $T_0$ ,  $T_p$  and  $T_{sp}$  are in  $^{\circ}\text{C}$ ,  $\chi_p$  in dry basis, and  $\dot{V}_{sp}$  in  $\text{m}^3 \text{h}^{-1}$ . The inlet air moisture content  $\chi_0$  is supposed constant here. Solving (32)–(36) by a fourth order Runge-Kutta (RK4) method with a 30 s sampling time, the state-space representation at discrete time  $k$  is:

$$\mathbf{x}(k+1) = \mathbf{f}(\mathbf{x}(k), \mathbf{u}(k)) \quad (37a)$$

$$\mathbf{y}_m(k) = \mathbf{x}(k) \quad (37b)$$

with  $\mathbf{y}_m$  and  $\mathbf{f}(\mathbf{x}, \mathbf{u})$  as the model output and state update function. The model state  $\mathbf{x}$  and input  $\mathbf{u}$  are defined as:

$$\mathbf{x}(k) = [T_0(k) \ \chi_p(k) \ T_p(k)]^T \quad (38)$$

$$\mathbf{u}(k) = [\dot{V}_{sp}(k) \ T_{sp}(k)]^T \quad (39)$$

### 2.6 Control algorithm

Model performances for control are demonstrated with an NMPC scheme based on an internal model structure, as illustrated in Fig. 2. Desbiens et al. (2000) describe a similar design, but for the linear case. At each control period  $k$ , the following optimization problem is solved:

$$\min_{\Delta \mathbf{U}} [(\hat{\mathbf{R}} - \hat{\mathbf{Y}})^T \mathbf{M}_{H_P} (\hat{\mathbf{R}} - \hat{\mathbf{Y}}) + (\Delta \mathbf{U})^T \mathbf{N}_{H_C} (\Delta \mathbf{U})] \quad (40)$$

with the input increments over the control horizon  $H_C$ :

$$\Delta \mathbf{U} = \begin{bmatrix} \Delta \mathbf{u}(k+0) \\ \Delta \mathbf{u}(k+1) \\ \vdots \\ \Delta \mathbf{u}(k+H_C-1) \end{bmatrix} \quad (41)$$

in which  $\Delta \mathbf{u}(k+j) = \mathbf{u}(k+j) - \mathbf{u}(k+j-1)$  for  $j = 0$  to  $H_C - 1$ . The predictions of the setpoint  $\mathbf{r}(k)$  and plant output  $\mathbf{y}(k)$  over the horizon  $H_P$  are:

$$\hat{\mathbf{R}} = \begin{bmatrix} \hat{\mathbf{r}}(k+1) \\ \hat{\mathbf{r}}(k+2) \\ \vdots \\ \hat{\mathbf{r}}(k+H_P) \end{bmatrix} \quad \text{and} \quad \hat{\mathbf{Y}} = \begin{bmatrix} \hat{\mathbf{y}}(k+1) \\ \hat{\mathbf{y}}(k+2) \\ \vdots \\ \hat{\mathbf{y}}(k+H_P) \end{bmatrix} \quad (42)$$

Table 1. Simplified model parameters for batch fluidized bed drying

parameter	value	standard deviation	units
$\chi_0$	$0.15 \times 10^{-2}$	–	–
$a_1$	$9.26 \times 10^{-5}$	$0.04 \times 10^{-5}$	$\text{m}^{-3}$
$b_1$	$4.54 \times 10^{-2}$	$0.05 \times 10^{-2}$	$^{\circ}\text{C} \text{m}^{-3}$
$b_2$	$2.56 \times 10^{-5}$	$0.02 \times 10^{-5}$	$\text{m}^{-3}$
$\nu$	3.48	0.12	–
$\chi_{pc}$	$2.33 \times 10^{-2}$	$0.06 \times 10^{-2}$	–
$\alpha$	$4.90 \times 10^{-3}$	–	–
$\beta$	$5.70 \times 10^{-2}$	–	$^{\circ}\text{C}^{-1}$
$\tau$	86.7	–	s

where  $\hat{\mathbf{r}}(k+j) = \mathbf{r}(k)$  and  $\hat{\mathbf{y}}(k+j) = \hat{\mathbf{y}}_d(k+j) + \hat{\mathbf{y}}_s(k+j)$  for  $j = 1$  to  $H_P$ . The weighting matrices  $\mathbf{M}_{H_P}$  and  $\mathbf{N}_{H_C}$  are:

$$\mathbf{M}_{H_P} = \text{diag}\{\mathbf{M}, \mathbf{M}, \dots, \mathbf{M}\} \quad (43)$$

$$\mathbf{N}_{H_C} = \text{diag}\{\mathbf{N}, \mathbf{N}, \dots, \mathbf{N}\} \quad (44)$$

with  $\mathbf{M}$  and  $\mathbf{N}$  as the setpoint tracking and input increment weights.

The  $H_P$  deterministic predictions  $\hat{\mathbf{y}}_d(k+j)$  are generated at time  $k$  by recursively calculating (37) from its current state  $\mathbf{x}(k)$ . The  $H_P$  stochastic predictions  $\hat{\mathbf{y}}_s(k+j)$  are obtained by forecasting the estimation of the current disturbance  $\mathbf{y}_s(k) = \mathbf{y}(k) - \mathbf{y}_m(k) = \mathbf{y}(k) - \mathbf{x}(k)$  over the future horizon. To do so, it is assumed that the disturbance is the result of filtering a zero mean white noise by a stochastic linear model  $\mathbf{G}_s$ . To ensure offset-free control,  $\mathbf{G}_s$  must contain an integrator for each controlled output. Additional poles and zeros modify the disturbance rejection dynamics as needed (Desbiens et al., 2000).

Problem (40) is solved with sequential quadratic programming (SQP) and constrained with:

$$\Delta \mathbf{u}_{\min} \leq \Delta \mathbf{u}(k+j) \leq \Delta \mathbf{u}_{\max} \quad j = 0, \dots, H_C - 1 \quad (45)$$

$$\mathbf{u}_{\min} \leq \mathbf{u}(k+j) \leq \mathbf{u}_{\max} \quad j = 0, \dots, H_C - 1 \quad (46)$$

$$\hat{\mathbf{y}}_{\min} \leq \hat{\mathbf{y}}(k+j) \leq \hat{\mathbf{y}}_{\max} \quad j = 1, \dots, H_P \quad (47)$$

## 3. RESULTS AND DISCUSSION

### 3.1 Model Calibration and Validation

The parameters of the simplified model require calibration. The heater closed-loop time constant  $\tau$  is already estimated for this equipment in Gagnon et al. (2020). A relative humidity measurement gives the inlet moisture content  $\chi_0$ . The exponential function  $\gamma$  of (14) is related to the saturation mixing ratio  $\chi_{\text{sat}}$ .  $\alpha$  and  $\beta$  parameters are therefore calibrated with exponential regression on data generated from physical considerations, using Dalton's Law for  $\chi_{\text{sat}}$ , and Tetens equation, for water vapor pressure. A regression from 20 to 60  $^{\circ}\text{C}$ , corresponding to typical  $T_p$  values, gives an excellent fit with a root mean square error (RMSE) on  $\chi_{\text{sat}}$  smaller than 0.05%. Table 1 gives  $\chi_0$ ,  $\tau$ ,  $\alpha$  and  $\beta$  calibrated values.

The grey-box identification estimates the remaining parameters:  $a_1$ ,  $b_1$ ,  $b_2$ ,  $\nu$  and  $\chi_{pc}$ . The algorithm is a non-linear least squares optimization problem minimizing the distance between simulated outputs and data, using parameters as decision variables. The model outputs in  $\mathbf{y}$

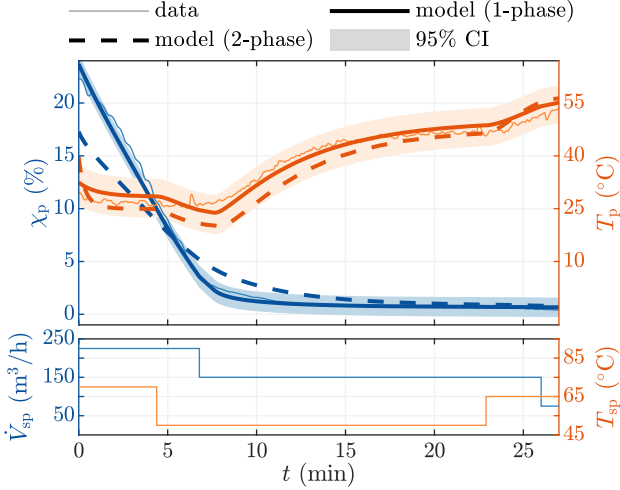


Fig. 3. Simplified 1-phase and complete 2-phase model comparison for batch B3

are weighted with  $\mathbf{w}$  in the least squares optimization algorithm:

$$\mathbf{w} = [0 \ 1.0 \ 0.004]^\top \quad (48)$$

by using the high limit of the measurement range and excluding  $T_0$  from calibration (already calibrated with  $\tau$ ). Four independent datasets are produced: B1 and B2 for calibration, and B3 and B4 for validation. The grey-box calibration is performed on B1 and B2 data, with a respective dry batch size of 3.91 kg and 3.78 kg (multiple experiment identification). Table 1 gives the identified parameters and their estimated standard deviation (highlighted in blue). The RMSE between model and calibration data are provided in Table 2, under 1-phase columns. The small RMSEs and standard deviations compared to estimated parameters, indicate a high confidence in the model with B1 and B2 data. Table 2 also include results with the complete two-phase description.

The model is cross-validated on B3 data, with experimental conditions similar to calibration (dry batch size of 3.98 kg). As shown by Fig. 3 and Table 2, B3 results suggest that predictive performances of the simplified single-phase model are better than the two-phase description. The simplifying assumptions however decrease extrapolation capabilities. In this regards, Fig. 4 and Table 2 compare both models with B4 data in which the batch size is 4.71 kg, thus significantly different from that used during calibration experiments. These results show that the simplified model displays sensitivity to variations in operating conditions for both outputs. Their two-phase counterparts do not exhibit the same limitation in robustness.

Table 2. Model adjustments for simplified 1-phase and complete 2-phase models

batch	usage	RMSE			
		$\chi_p$ (%)		$T_p$ (°C)	
		1-phase	2-phase	1-phase	2-phase
B1	calib.	0.5109	1.3095	2.5872	2.6176
B2	calib.	0.3780	1.2149	1.0154	3.2896
B3	valid.	0.4831	1.5435	1.8955	3.8632
B4	valid.	3.2358	1.3264	7.7996	2.6360

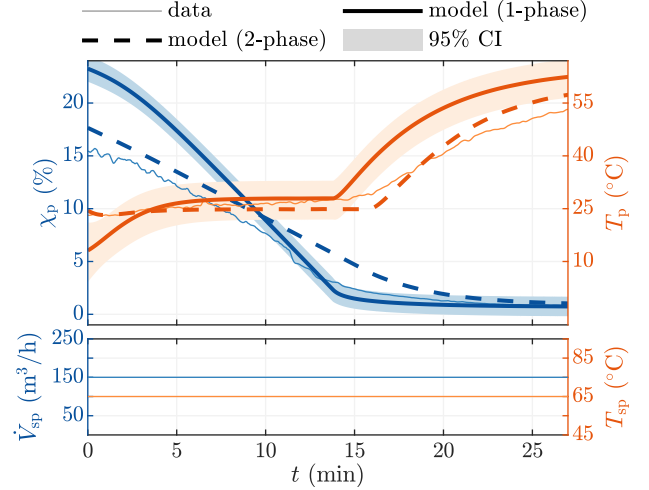


Fig. 4. Simplified 1-phase and complete 2-phase model comparison for batch B4

Model extrapolation capabilities are obviously affected by the fixed batch size hypothesis, but also by neglecting bubbles, since a single-phase is generally less representative of FBD operations (Dry and Judd, 1985). Note that batch size variations are generally not significant in production conditions. Colored areas around simulated outputs of Figs. 3 and 4 depict the estimated 95% confidence interval (CI), assuming a Gaussian distribution. These results show that the confidence in  $T_p$  is lower than  $\chi_p$ , presumably attributed to the adiabatic process hypothesis. Intervals are also wider in B4 than B3, confirming the lower model performance for B4 data. Notwithstanding limitations, the following results show that it can still be used for control applications as FBD general trends are conserved.

### 3.2 Predictive Control

The NMPC strategy described in Section 2 is applied on the complete two-phase FBD model with additive measurement noises. It is worth mentioning that the mismatches in the controller model (1-phase) and process model (2-phase), visible in Figs. 3 and 4, show the robustness of the proposed scheme. Knowing that the goals are to reach 1% moisture content while maintaining particle temperature below 45 °C, the control parameters are:

- control period : 30 s
- $H_P = H_C = 30$
- $\mathbf{r}(k) = [0 \ 0.01 \ 0]^\top$
- $\mathbf{M} = \text{diag}\{0, 1, 0\}$  and  $\mathbf{N} = 10^{-3} \text{diag}\{1, 0.4\}$
- $\Delta \mathbf{u}_{\min} = [-25 \ -10]^\top$  and  $\Delta \mathbf{u}_{\max} = [25 \ 10]^\top$
- $\mathbf{u}_{\min} = [75 \ 40]^\top$  and  $\mathbf{u}_{\max} = [200 \ 90]^\top$
- $\hat{\mathbf{y}}_{\min} = [-\infty \ -\infty \ -\infty]^\top$  and  $\hat{\mathbf{y}}_{\max} = [\infty \ \infty \ 45]^\top$

Note that the selected  $\mathbf{M}$  implies that only the moisture content is requested to follow a setpoint. Large  $H_P$  and  $H_C$  values are required to cover the whole batch and allow full flexibility on manipulated variables. Input constraints ensure appropriate product fluidization and inlet temperatures. The stochastic model is:

$$\mathbf{G}_s(q^{-1}) = \frac{(1 - 0.65q^{-1})^2}{1 - q^{-1}} \begin{bmatrix} \frac{1}{1-0.3q^{-1}} & 0 & 0 \\ 0 & \frac{1}{1-0.95q^{-1}} & 0 \\ 0 & 0 & \frac{1}{1-0.3q^{-1}} \end{bmatrix}$$

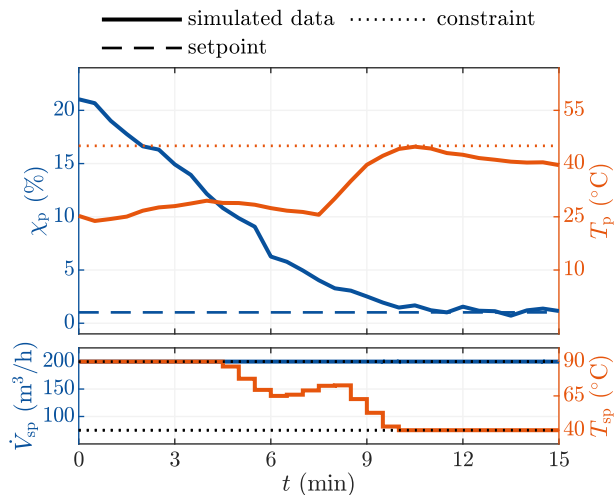


Fig. 5. Simplified predictive control results on simulator

where  $q^{-1}$  is the backshift operator.

Fig. 5 shows that the suggested control algorithm is able to reach the moisture setpoint and avoid particle overheating by using the imperfect single-phase model for predictions. To do so, the inlet temperature setpoint  $T_{sp}$  is decreased at the end of the batch while the airflow  $\dot{V}_{sp}$  is kept at its maximum, since its impact on the falling rate period is low. The simple predictive model, the single optimization routine of the NMPC and the absence of a nonlinear observer make the implementation and tuning easier than in Gagnon et al. (2017). The simpler formulation also allows a control period twice shorter.

At  $t = 7$  min, the  $T_{sp}$  increase is caused by modeling errors, particularly the fastest drying time of the simplified model, as depicted in Figs. 3 and 4. Through feedback, the NMPC compensates for model mismatches, ensuring adequate drying at the end of the batch. The only cost is a marginally suboptimal cycle time, since a strategy based on the two-phase equations would decrease the temperature slightly later in the batch.

#### 4. CONCLUSION

This work derives a single-phase batch fluidized bed dryer model for nonlinear model predictive control. The simplifying assumptions introduced allow representing the dynamics with five equations. Process parameters are calibrated with grey-box identification from pilot scale experimental data. The predictive control algorithm uses an internal model structure with linear stochastic predictions. Validation and control results with the complete two-phase description indicate that the proposed simplifications do not impair the ability to adequately replicate the process dynamics, and is thus suitable to design predictive control laws. The higher level of empiricism however reduces model extrapolation capabilities. Nevertheless, the closed-loop performances display robustness to modeling errors.

Future works will tackle the issue of fluctuating inlet air moisture content with feedforward control, and study alternative approaches such as sliding mode control, to further ease the implementation. Other applications also include moisture soft sensing based on state observers.

#### ACKNOWLEDGEMENTS

The authors would like to thank Pfizer Montreal and the National Sciences and Engineering Council of Canada (NSERC) for funding this research, and Pfizer Canada ULC for providing the necessary raw materials and laboratory equipment.

#### REFERENCES

- Burgschweiger, J., Groenewold, H., Hirschmann, C., and Tsotsas, E. (1999). From hygroscopic single particle to batch fluidized bed drying kinetics. *The Canadian Journal of Chemical Engineering*, 77(2), 333–341.
- Desbiens, A., Hodouin, D., and Plamondon, É. (2000). Global predictive control: a unified control structure for decoupling setpoint tracking, feedforward compensation and disturbance rejection dynamics. *IEE Proceedings - Control Theory and Applications*, 147(4), 465–475.
- Dry, R.J. and Judd, M.R. (1985). Fluidised beds of fine, dense powders: scale-up and reactor modelling. *Powder Technology*, 43(1), 41 – 53.
- Gagnon, F., Bouchard, J., Desbiens, A., and Poulin, É. (2020). Development and validation of a batch fluidized bed dryer model for pharmaceutical particles. *Drying Technology*, 1–24.
- Gagnon, F., Desbiens, A., Poulin, É., Lapointe-Garant, P.P., and Simard, J.S. (2017). Nonlinear model predictive control of a batch fluidized bed dryer for pharmaceutical particles. *Control Engineering Practice*, 64, 88–101.
- Gavi, E. (2019). Application of a mechanistic model of batch fluidized bed drying at laboratory and pilot scale. *Drying Technology*, 1–17.
- Kunii, D. and Levenspiel, O. (1991). *Fluidization engineering*. Butterworth Heinemann, 2nd edition.
- Martinez-Vera, C., Vizearra-Mendoza, M., Galin-Domingo, O., and Ruiz-Martinez, R. (1995). Experimental validation of a mathematical model for the batch drying of corn grains. *Drying Technology*, 13(1-2), 333–350.
- Mujumdar, A.S. (2014). *Handbook of industrial drying*. CRC Press, 4th edition.
- Nagy, Z.K. and Braatz, R.D. (2003). Robust nonlinear model predictive control of batch processes. *AIChE Journal*, 49, 1776–1786.
- Philippesen, C.G., Vilela, A.C.F., and Zen, L.D. (2015). Fluidized bed modeling applied to the analysis of processes: review and state of the art. *Journal of Materials Research and Technology*, 4(2), 208–216.
- Syahrul, S., Dincer, I., and Hamdullahpur, F. (2003). Thermodynamic modeling of fluidized bed drying of moist particles. *Int. J. of Thermal Sciences*, 42(7), 691 – 701.
- van Meel, D.A. (1958). Adiabatic convection batch drying with recirculation of air. *Chemical Engineering Science*, 9(1), 36 – 44.
- Yang, W. (2003). *Handbook of Fluidization and Fluid-Particle Systems*. Chemical Industries. Taylor & Francis.